Indonesian Journal of Pharmacy

VOL 34 (3) 2023: 471–481 | RESEARCH ARTICLE

# Alginate-ZnO-Poly(ethylene glycol) dimethacrylate (PEGDMA) via Interpenetrating Polymer Network as a Functional Material for Wound Dressing

**Ane Nurjanah*, Muhammad Bachri Amran, and Rusnadi**

Department of Chemistry, Faculty of Mathematics and Natural Science, Institut Teknologi Bandung, Bandung, Indonesia

**Article Info**

**Submitted:** 20-08-2022
**Revised:** 02-04-2023
**Accepted:** 08-08-2023

*Corresponding author
Ane Nurjanah

Email:
ane_nurjanah@students.itb.ac.id

**ABSTRACT**

Alginate is a common biopolymer used as a wound dressing material. Nanoparticles and synthetic polymers are used to modify alginate to increase the mechanical and antibacterial properties of a wound dressing material, such as ZnO. It has potential in medical applications due to its good antibacterial properties. In contrast, PEGDMA has not been widely used in the medical field, so it has the potential to be developed as wound dressing materials. However, there is no detailed report on the modification of alginate using ZnO and poly(ethylene glycol) dimethacrylate (PEGDMA). In this paper, alginate (A) was modified using ZnO (Z) and PEGDMA (P) (AZP) through the interpenetrating polymer network (IPN) method. AZP could increase a wound dressing material's mechanical property by 78%. It also showed antibacterial properties of 94%, which indicated that the modified alginate with ZnO and PEGDMA had a high-performance wound dressing material.

**Keywords:** wound dressing material, alginate, ZnO nanoparticle, PEGDMA, Interpenetrating Polymer Network (IPN).

## INTRODUCTION

Wounds occur as an impact of the damage in the body's structure or function due to physical or chemical force or pressure. The first aid for wounds is the use of wound dressing materials. Biopolymer has the potential as wound dressing material, but it lacks mechanical and antibacterial properties when applied to wound dressing materials (Khalid, *et al*., 2017; Mahdavi, *et al*., 2013; Wang *et al*., 2016; Wang, *et al*., 2016). Alginate is a biopolymer that has received great attention in the medical field but exhibits low mechanical and antibacterial properties for wound dressing materials (Branco da Cunha *et al*., 2014; Foliatini, *et al*., 2015; Khalid *et al*., 2017). Synthetic polymers such as poly(vinyl alcohol) (Lam, *et al*., 2017), poly(ethylene glycol) (Branco da Cunha *et al*., 2014), and poly(ethylene glycol) methacrylate (PEGMA) modified with biopolymers have been widely used as wound dressing materials to improve mechanical and antibacterial properties (Khalid *et al*., 2017).

One method that has been used for producing wound dressing materials is the Interpenetrating Polymer Network (IPN). The IPN method offers a simple mixing technique. However, it produces a strong polymer material due to the two or more crosslinked networks that are difficult to separate (Khalid *et al*., 2017). Previous studies have shown that hydrogel nanocomposites with an IPN structure increased the mechanical strength and antibacterial properties of wound dressing materials due to crosslinking interactions in the tissue (Khalid *et al*., 2017). Hence, modification is required to improve alginate performance as a wound dressing material, such as combining it with synthetic polymers to form composite materials. This study used poly(ethylene glycol) dimethacrylate (PEGDMA) as the modifier. Synthetic polymers usually have a crosslinked network that can be interpreted into the alginate network to strengthen the material formed. The crosslinked network of PEGDMA, which is interpenetrated into the alginate, can improve the mechanical resistance properties of the IPN material. Indeed, the crosslinked bond between PEGDMA and alginate improves the mechanical resistance properties of IPN materials.

Regarding enhancing the antibacterial properties of wound dressing materials, some previous research mainly reported ZnO as the most effective additive material (Khalid *et al*., 2017; Lam *et al*., 2017; Sehmi *et al*., 2016). It is interesting to

investigate the improvement contributed by the addition of ZnO to alginate–PEGDMA composites, which has never been reported. Moreover, detailed studies on the effect of using IPN with modified alginate and ZnO–PEGDMA on the mechanical strength and antibacterial properties of wound dressing materials have not been carried out, which makes this research necessary. IPN can process alginate as a wound dressing material to enhance mechanical and antibacterial properties. Two crosslinked networks are required to form IPN, which can be obtained from alginate and synthetic polymers.

Based on the previous study (Branco da Cunha *et al*., 2014; Foliatini *et al*., 2015; Khalid *et al*., 2017; Lam *et al*., 2017; Sehmi *et al*., 2016), it is interesting to investigate the use of ZnO-PEGDMA interpenetrated with alginate to improve the mechanical resistance and antibacterial properties of the wound dressing material. Therefore, in this paper, alginate modification with ZnO and PEGDMA will be carried out as a candidate for wound dressing material.

## MATERIAL AND METHODS

The materials used were sodium alginate with viscosity $10^4$ µg/mL at 20°C (Wako 1st Grade Pure Chemical Industries, Ltd., Osaka, Japan), ethylene glycol dimethacrylate (EGDMA; Sigma-Aldrich, St. Louis, MO, USA), zinc nitrate hexahydrate ($Zn(NO_3)_2.6H_2O$; Merck Chemical Company, Darmstadt, Germany), sodium hydroxide (NaOH; Merck), and biphenyl oxide (BPO; Merck), and nitrogen gas (PT. Aneka Gas Industri; Bandung, Indonesia). *Escherichia coli* ATCC 25922 and *Staphylococcus aureus* ATCC 25923 isolates were obtained from the Medical Laboratory Technology Type Culture Collection (Bandung Health Polytechnic, Bandung, Indonesia).

### Synthesis and characterization of ZnO

ZnO synthesis was carried out using the sol–gel method using sodium alginate reagent. Each solution of $Zn(NO_3)_2.6H_2O$ (0.034 mM) and sodium alginate (1% (w/v)) was prepared in 250 mL of water. The primary solution of $Zn(NO_3)_2.6H_2O$ and sodium alginate was diluted to 1.000 µg/mL and 2.000 µg/mL, respectively, to as much as 50 mL. The $Zn(NO_3)_2.6H_2O$ and sodium alginate solution were mixed using a magnetic stirrer at 50°C and 700 rpm. The mixture was then centrifuged to separate the solid gel and the filtrate. The ZnO solid particles obtained from a solid gel were calcined for 1 h using a furnace at a temperature of 700°C. The result was ZnO(1). On the other hand, the second synthesis of ZnO (ZnO (2)) performed the precipitation method by reacting zinc nitrate with sodium hydroxide without calcination (Chiang & Chu, 2015). The yield of ZnO was determined with equation 1.

$$\frac{Mass\ of\ synthesized\ ZnO\ (mg)}{Mass\ ZnO\ (NO_3)2.6H_2Omg)}\ x\ 100\% \quad \text{..... (1)}$$

The ZnO solid particle obtained from the previous step was characterized for its functional group using Fourier Transform Infrared (FTIR), Shimadzu, type IR Prestige 21 by employing KBr disk technique. The spectra were taken between 400 – 4000 $cm^{-1}$ range with a resolution of 2 $cm^{-1}$. X-Ray Diffraction (XRD) was performed to determine ZnO crystallinity. XRD measurements at room temperature were performed with a Bruker D8 Advance using Cu Kα radiation ($\lambda$ = 0.1541 nm) in the scanning range 2θ of 10° – 80°. SEM-EDX (SEM SU3500) was carried out to analyze surface morphology, particle size, and the elemental composition of ZnO. The observation was carried out in the range of 2000 – 40.000 magnification. Standard mass percentage was obtained from a database that refers to the ZAF Method Standardless Quantitative Analysis (Schwartz *et al*., 2009).

### Synthesis and characterization of alginate–ZnO–PEGDMA (AZP) material

The sodium alginate, ZnO, and EGDMA were added with 50 mL of acetonitrile and left to stand for 2 h at 25°C. The mixture was sonicated (frequency: 42 kHz) for 1 h. Then, it was added with 100 mg of BPO as the initiator. The mixture was flowed with nitrogen gas for 15 min and then heated in an oven at a temperature of 70°C–80°C. It was observed for every 2 h until hydrogel was formed. The hydrogel was dried at 25°C by casting to obtain a dry hydrogel.

### Mechanical properties testing of the AZP material

The mechanical properties were analyzed using a Favigraph, a tool to measure tensile strength, with a clamp distance of 2.5 mm and a tensile speed of 10 mm/min to determine the performance of these materials. The two samples were tested, i.e., Alginate-ZnO (AZ) and AZP. The sample was gel dried into thin films and cut with a length of 3 cm and a width of 0.2 cm. Each sample

has three variations of concentrations. The sample was tested sequentially, starting from AZ-1, AZ-2, to AZ-3, then AZP-1, AZP-2, and AZP-3 (Supplementary Materials).

**Study of the antibacterial properties of the AZP material**

The antibacterial test was performed to evaluate the antibacterial activity against common pathogens in wound infection. In this study, gram-negative bacteria species, *Escherichia coli* (*E. coli*) and gram-positive bacteria *Staphylococcus aureus* (*S. aureus*), were used with Mannitol Salt Agar (MSA) media. Samples were cut to a size of 20 mm. Ciprofloxacin was used as a standard drug (positive control). The sample was placed on a plate and incubated at 37°C for 24h. The zone of inhibition was measured to determine the antibacterial properties of Alginate-ZnO (AZ) and Alginate-ZnO-PEGDMA (AZP). The percentage of inhibition was determined using equation (2), as proposed in a previous study (Khalid *et al*., 2017):

$$\text{Percent inhibition} = \left( \frac{\text{Zone of inhibition of test sample (mm)}}{\text{Zone of inhibition of standard drug (mm)}} \right) \times 100 \quad \text{.....(2)}$$

## RESULTS AND DISCUSSION

### Synthesis and Characterization of ZnO nanoparticles

### Synthesis of ZnO nanoparticles

The synthesis resulted in ZnO(1) and ZnO(2) in the form of white powder, but the color of the ZnO (1) solid was duller than ZnO (2), considering the first ZnO synthesis required a very high calcination temperature. ZnO (1) required a shorter time, but ZnO (2) was simpler because it did not require high temperatures. The yields of ZnO (1) and (2) were 11.95% and 29.04%, respectively. The yield percentage of ZnO (1) was smaller than ZnO (2). However, the use of sodium alginate in ZnO (1) was preferable for its application as a wound dressing due to its properties of alginate that biodegradability, biocompatibility, and accessibility. Alginate contains 70% water by volume that can absorb the exudate secreted from the wound (Agarwal *et al*., 2011; Wang *et al*., 2016; Alavi *et al*., 2019). The $Zn(NO_3)_2.6H_2O$ used in ZnO (2) was twice more than zinc nitrate in ZnO (1), so the yield percentage of ZnO (2) was also about twice compared to ZnO (1). The mass of $Zn(NO_3)_2.6H_2O$ used in ZnO (2) was 6.29 g, while the mass of $Zn(NO_3)_2.6H_2O$ in ZnO (1) was 2.5 g.

### Characterization of ZnO nanoparticles using FTIR

The purity level of ZnO nanoparticles from ZnO (1) and ZnO (2) was characterized by FTIR and XRD. It generally shows a significant absorption area at 800–1200 $cm^{-1}$. The sharp peaks at wavenumbers 445.20 $cm^{-1}$ and 447.49 $cm^{-1}$ demonstrated the presence of ZnO. Meanwhile, the strong and broad absorption at wavenumbers 3450.65 $cm^{-1}$ and 3425.58 $cm^{-1}$ were identified as O–H vibrations from trapped $H_2O$. It explained the hygroscopic properties of this material (Iwamura, *et al.,* 2016). The possibility of $Zn(OH)_2$ residues was shown by O-H peak at wavenumbers 3425 $cm^{-1}$ and 3450 $cm^{-1}$ (Figure 1). Also, O–H bending vibrations from $H_2O$ were present at 1435.04 $cm^{-1}$ for ZnO (1), while 1625.99 $cm^{-1}$ and 1382.90 $cm^{-1}$ for ZnO (2).

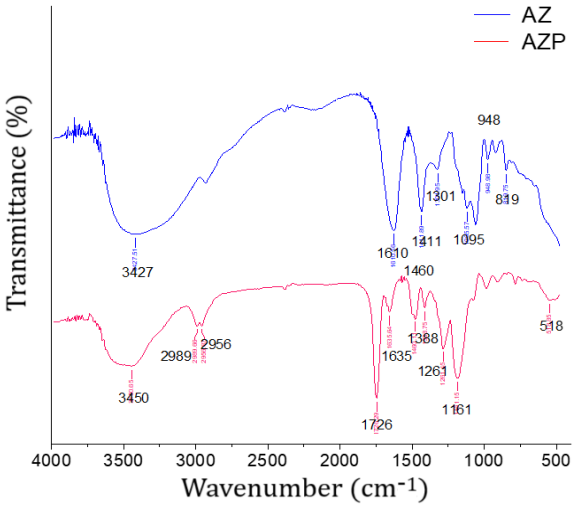


Figure 1. The IR spectra of Alginate-ZnO (AZ) and Alginate–ZnO–PEGDMA (AZP)

The heating factor can change the material structure's shape, the crest's sharpness, and the wavenumber shift. FTIR spectrum character of ZnO (1) was more dominant than ZnO (2), indicated by the shifting of wavenumbers and the appearance of two peaks in ZnO (2), whereas ZnO (1) only produced one peak. ZnO (1) was sharper than ZnO (2) due to the high heating factor on ZnO (1). A high heating factor can produce a higher purity level indicated by peak sharpness (Wang *et al*., 2016). ZnO(2) gave a shift in wavenumber and reduced the sharpness, exposing the purity level reduction. Based on FTIR results, the information regarding the purity of ZnO was still questionable. Therefore, ZnO (1) and ZnO (2) nanoparticles were characterized using XRD.

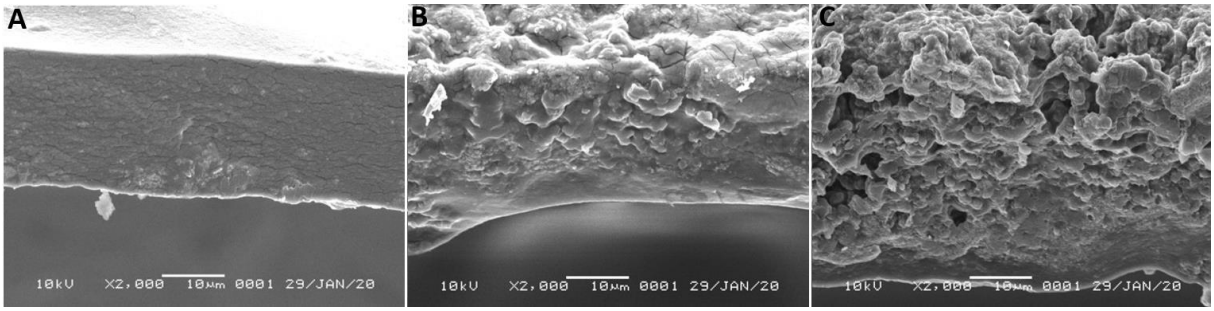


Figure 2. Morphology of Alginate–ZnO–PEGDMA (AZP): Morphology of AZP-1 (a); Morphology of AZP-2 (b); Morphology of AZP-3 (c) at 2000x magnification

**Characterization of ZnO nanoparticles using XRD**

The XRD analysis of ZnO showed that ZnO (1) and (2) had standard ZnO crystal lattice. The XRD peaks were at the position of 31.82°, 34.47°, 36.19°, 47.57°, 56.78°, and 62.73° corresponding to the lattice planes (1 0 0), (0 0 2), (1 0 1), (1 0 2), (1 1 0), and (1 1 0). The crystal structure of ZnO was wurtzite (Figure 2) and similar to the previous study (Gu, *et al.,* 2011). It was indicated by XRD peaks that matched ZnO's standard hexagonal wurtzite structure (ICDD 00-003-0888). The wurtzite structure is the most stable at room temperature and pressure (Lam *et al.,* 2013). The hexagonal shape has two sublattices, $Zn^{2+}$ and $O^{2-}$, alternately forming the base plane. The tetrahedral atom arrangement in the wurtzite structure is noncentrosymmetric, which creates a dipole moment (Marinho *et al*., 2012). It is a determining factor for some of the properties of the ZnO nanoparticles. Thus, the ZnO (1) and ZnO (2) synthesized results are pure. Based on these results, ZnO nanoparticles have been successfully synthesized. The highest crystal intensity value (36.19°) in ZnO (1) was greater than ZnO (2) due to the use of sodium alginate, which can increase the volume of ZnO crystals to increase crystallinity (Khalid *et al*., 2017; Wang *et al.*, 2016).

**Characterization of ZnO nanoparticles using SEM-EDX**

The morphology percentage of elements in ZnO (1) and (2) nanoparticles were observed using SEM-EDX, while the particle size distribution was analyzed by PSA as supporting data. The morphology of ZnO (1) and (2) nanoparticles was observed at magnifications of 20000x and 40000x, respectively. The distribution of ZnO appeared to have a non-uniform shape. It is because the entire sample experienced agglomeration between the ZnO particles. SEM imaging shows that the ZnO obtained was generally spherical, with clearly visible gaps between particles (Al-Sabahi, *et al.*, 2018). At a magnification of 40.000x, the ZnO particle size scale could be observed. The particles of ZnO (1) were 53–82 nm, and ZnO(2) were 71–376 nm. The heating factor affected the ZnO particle size scale. The heating in the synthesis process of ZnO (1) was much higher than ZnO (2). The high heating temperature during synthesis causes the ZnO particle size to shrink (Wang *et al*., 2016). The results were similar to Romadhon *et al*. Temperature plays an essential role in reducing particle size. In higher temperatures, ZnO has a smaller size of nanoparticles (Romadhon *et al*., 2016).

The characterization of the samples using the EDX instrument showed that ZnO (1) and (2) contained Zn and O elements with atomic and mass percentage ratios close to the standard Zn and O percentages referred to (Table III in Supplementary Materials). These results support that the ZnO synthesized was pure. The following is the data from the synthesized ZnO analysis using EDX instrument. The results of the EDX show that ZnO (1) had a mass% close to the standard mass% of ZnO. The heating factor was the main factor of this phenomenon (Jafarirad, *et al.*, 2016).

**Synthesis and characterization of the AZP material**

Synthesis and characterization of AZP were carried out in two stages. The first step was to synthesize AZ material, which showed good antibacterial activity for wound dressing use. BPO initiated the polymerization process in converting EGDMA into a radical molecule which underwent a chain extension stage to produce PEGDMA. Furthermore, PEGDMA was selected as a synthetic polymer to synthesize this alginate-based IPN material to have good mechanical resistance properties. PEGDMA has a crosslinked network, so

it is expected that the mechanical resistance properties of the IPN material can be improved. The requirement for the formation of an IPN is there are at least two crosslinks. Alginate already has crosslinks and the second crosslinking resulted from the modification of alginate with PEGDMA. The role of PEGDMA as a crosslinker can be interpenetrated into alginate molecules so that IPN material can be formed (Wang *et al.*, 2017). PEGDMA has been used in medical applications, but as a synthetic polymer in wound dressing materials has never been done. Meanwhile, Wang (2016) used a synthetic polymer of poly (ethylene glycol) methacrylate (PEGMA) modified with agarose and ZnO to produce wound dressing materials. The result is that PEGMA modification can increase the mechanical resistance properties of the IPN materials. The amount of alginate, ZnO, and EGDMA used to synthesize this IPN material were 1 mmol, 4 mmol, and 20 mmol. The synthesized AZP material was obtained as white powder of as much as 4.9959 g. Furthermore, the Alginate-ZnO-PEGDMA (AZP) membrane and its comparison of Alginate-ZnO (AZ) were varied in concentration to evaluate the physical form and performance of each. Variations in AZ and AZP materials concentration were made into 3, namely AZ-1, AZ-2, and AZ-3. The composition of alginate was made the same, and the composition of ZnO was made different with a ratio of 1: 3: 5. Likewise with AZP materials. The variation of the concentration of AZP material is made into 3, namely AZP-1, AZP-2, and AZP-3. The characterization of AZP material was performed using FTIR and SEM-EDX.

The results show the O–H function group at the wavenumber absorption of 3448.72 $cm^{-1}$ for the AZ material. There was a decrease in the intensity of the wavenumber at 3427.51 $cm^{-1}$ when interacting with PEGDMA. In addition, the functional groups C=C at 1622.13 $cm^{-1}$ experienced a shift to 1600.92 $cm^{-1}$ for the AZP material. The presence of ZnO in the AZ material showed more absorption and shifting of wavenumbers at 1170 $cm^{-1}$ and 1018.41 $cm^{-1}$ because of the interaction with PEGDMA had occurred. The interactions were semi-IPN non-covalent. PEGDMA has crosslinks that interact with ZnO first. Then ZnO-PEGDMA would interpenetrate into the polymer system from alginate. The presence of PEGDMA indicated the formation of IPN. It can be seen in the COO- (carboxyl) functional group at 1726.29 $cm^{-1}$. The AZP material was confirmed through FTIR data where there was no BPO functional group (benzoyl and peroxide). BPO disappeared when the gel has formed because the half-life of BPO is only about 1h of heating.

The presence of PEGDMA significantly can be seen in the absorption of COO- at a wavenumber of 1726.29 $cm^{-1}$, while its interaction with AZ material was indicated by shifting some of its main peaks, including 1635.64 $cm^{-1}$, 1460.11 $cm^{-1}$, 1386.75 $cm^{-1}$, 1261.45 $cm^{-1}$, and 1161.15 $cm^{-1}$. The peak of C=C alkene from AZ material experienced a shift in wavenumber. Its intensity was decreased at 1635.64 $cm^{-1}$, indicating that PEGDMA has interacted with AZ. The presence of PEGDMA affected the absorption of the O-H group on the AZ material as a result of the interaction between AZ molecules and PEGDMA at 1460.11 $cm^{-1}$ and 1386.75 $cm^{-1}$. The interaction of PEGDMA with AZ material was more dominant, shown by the shifting of important groups of AZ material, such as C-O-C ether at 1095.57 $cm^{-1}$ shifted to 1261.45 $cm^{-1}$ and the shifting of ZnO at 1095.57$cm^{-1}$ to 1161.15 $cm^{-1}$.

The morphology, particle size distribution, and analysis of the percentage of elements present in the synthesized AZP were observed using SEM-EDX. The morphology of AZP material was successfully observed at magnifications of 2000x (Figure 3). The SEM imaging results show that the synthesized AZP has a spherical "flower-like" shape with the gaps between the particles (Figure 3A). The flower-like morphology of AZP is likely because of ZnO nanoparticles, which have several petals that grow radially from the center and are well dispersed (Lam *et al*., 2017). At a magnification of 40000x, the AZP particle size scale can be observed as 105–171 nm (Figure 3c). The particle size distribution was not uniform, but the size range was not too different (under 200 nm), indicating that the AZP material's constituent components were quite well dispersed. The difference in size was caused by agglomeration. Agglomeration can reduce the distribution of particle sizes, so the range of particle sizes will be farther apart. Agglomeration can be prevented by selecting the appropriate solvent: polar/non-polar solvents for hydrophilic/hydrophobic samples, low sample concentrations, and re-despiration using ultrasonic (Khalil, 2017).

The agglomeration between the constituent components of AZP occurred due to the influence of polarity, electrostatic power between particles, and large energy on the surface of the sample, which usually occur during the synthesis (Lam *et al*., 2013; Mahdavi *et al*., 2013; Wang *et al*., 2016).

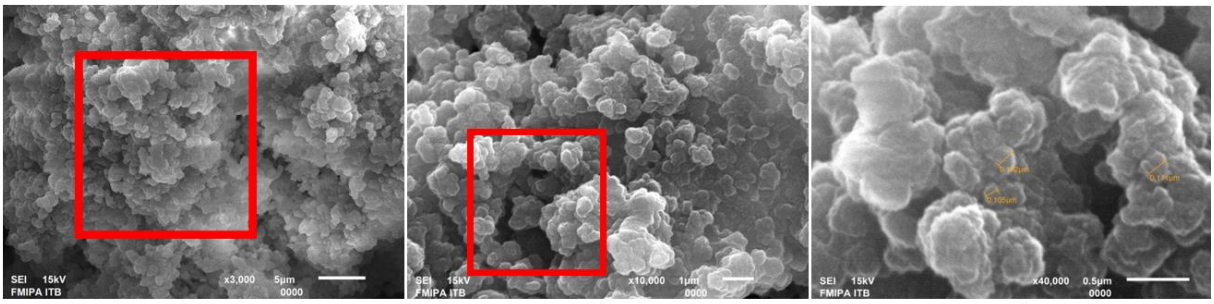


Figure 3. Morphology of AZP-2 at 3000x magnification (a), 10.000x magnification (b), and 40.000x magnification (c)

The size of the ZnO particles produced is highly dependent on the size of the traps surrounding the surface of the nanoparticles (Foliatini *et al*., 2015). The resulting AZP particle size distribution varied within the range (105–171 nm). Particles with diameter of <1000 nm can be accepted as nano-sized carriers used in the pharmaceutical industry (Vasquez *et al*., 2016). Synthesizing materials using natural materials is greatly influenced by concentration. The greater the alginate concentration, the greater the average AZP particle size produced (Wang *et al.,* 2016). This tendency is because the greater the alginate concentration, the more functional groups available to reduce metal ions (Guo *et al.,* 2011). The reduction of $Zn^{2+}$ to ZnO occurred in the calcination step. The reduction reaction was shown in Equation 3 and 4 (Nurbayasari *et al*., 2017). It results in forming a large number of particles so that the distance between the particles gets smaller, thus allowing the interaction between particles to form particles with a larger size.

$2Zn(OH)_{2(s)} \rightleftharpoons Zn^{2+} + 2OH^-$ .....(3)

$Zn^{2+} + 2OH^- \rightleftharpoons ZnO_{(s)} + H_2O$ .....(4)

AZP characterization using the EDX instrument showed that the synthesized AZP contained C, O, and Zn, with a mass percentage ratio close to the standard percentages for C and Zn. At the same time, for O, the difference was quite wide. AZP material was successfully analyzed at 3000x magnification. The mass percentage of C was quite close to the standard mass percentage (Table IV in Supplementary Materials). C was obtained from alginate and PEGDMA. The concentration of alginate and PEGDMA used in the synthesis process of the AZP material was greater when compared to ZnO. The mass percentage of Zn was close to the standard mass percentage, only within a very small range of 0.05%. The proximity factor of this result was the effectiveness of using ZnO nanoparticles during the synthesis process. ZnO will interact first with PEGDMA and then be interpenetrated into alginate molecules so the atomic mass of Zn in AZP material is relatively the same as the atomic mass of Zn in ZnO nanoparticles. The concentration of ZnO used was 4 mmol or about 0.3266 g. O displays a high range of differences in the percentage of its standard mass. It is probably because there is still much oxygen during the AZP material synthesis process. In addition, there are many O in PEGDMA since the concentration of PEGDMA used for the synthesis process is relatively high (Shalumon, *et al.,* 2011).

**Study of the mechanical properties of the AZP material**

Figure 5 shows the tensile strength values of AZ and AZP. AZP material exhibited higher tensile strength values than AZ material. Alginate is a biopolymer that can be applied as a wound dressing material (Shalumon *et al*., 2011). Alginates can form gels, but the disadvantage of this application is their low mechanical resistance properties (Chiang & Chu, 2015). The use of PEGDMA in this research could improve the mechanical resistance properties of alginate. AZP material exhibited higher mechanical resistance properties when compared with AZ. The interpenetration of PEGDMA into AZ improved the overall mechanical performance. The improved mechanical properties of the AZP material could be attributed to the favorable interaction between the alginate and ZnO–PEGDMA crosslinks in the network. The improvement in tensile strength was mainly due to crosslinked network inter-penetration between ZnO-PEGDMA and alginate.

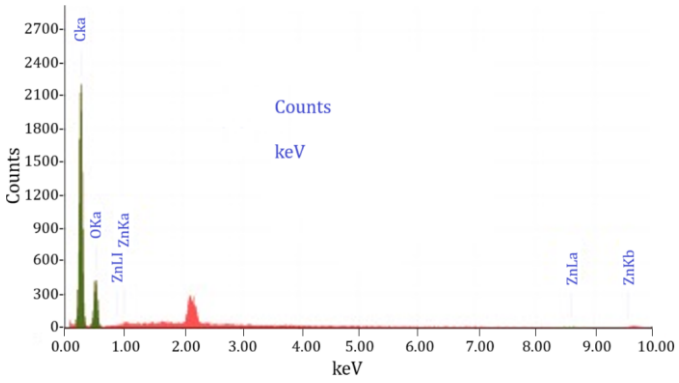


Figure 4. The results of EDX analysis of Alginate-ZnO-PEGDMA (AZP-2)

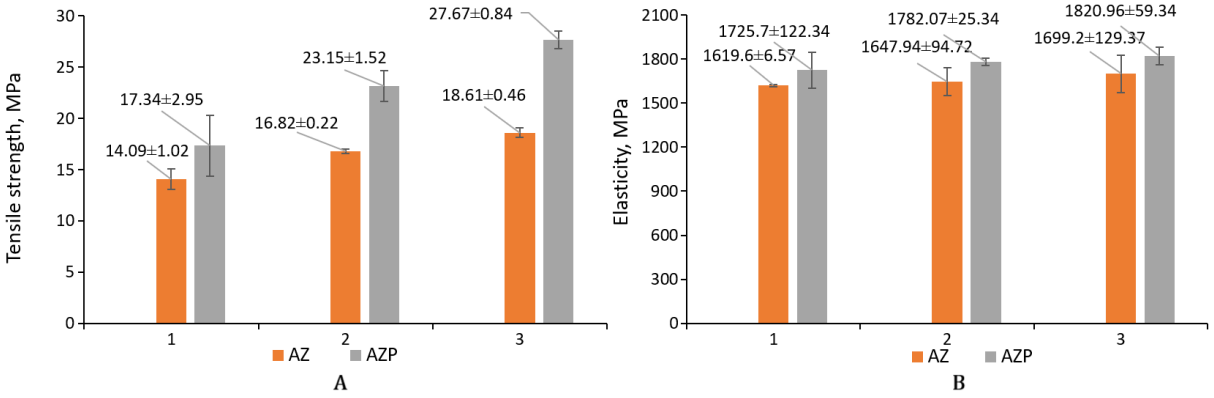


Figure 5. The tensile strength (a) and the elasticity (b) value of AZ and AZP materials

Likewise, the higher AZP elasticity value compared to AZ was caused by two crosslinked networks that made the AZP material less prone to fracture (Wang *et al*., 2016). Moreover, the synthesis process of IPN may affect its ability to strengthen the polymer, which leads to producing a solid material. In previous research, the agarose composite only showed moderate tensile strength, while adding ZnO–PEGMA significantly improves this composite (Wang *et al*., 2016).

Tensile strength is the maximum stress a material can withstand when stretched or pulled before it breaks. In its application, tensile strength is used to design a part of a ductile, brittle, and not static structure. In short, it always receives a large amount of force even though the object is not moving. For wound dressing materials, tensile strength affects the product quality because dressing materials should not be allowed to break concerning load or deformation (Pavlina and Tyne, 2008; Sun *et al*., 2017). For example, if the wound dressing material is a membrane, the membrane that is not easily broken would be preferred by a consumer versus the membrane that is easily broken. Likewise, a gel that does not easily melt is preferable to a thin gel. The tensile strength of the IPN material is greatly influenced by the basic properties of the polymer itself (Chiang and Chu, 2015). Adding PEGDMA to tensile strength can improve the mechanical resistance properties of the IPN material (Wang *et al*., 2016). PEGDMA acts as a crosslinking agent that can increase tensile strength and the IPN material's elasticity by increasing the covalent bonds between polymers. When mixed into the polymer, it will microscopically affect a material's mechanical resistance properties (Mowade, *et al.,* 2012).

Figure 5 presents the elasticity values of the AZ and AZP materials. The elasticity of AZP displayed a higher value than AZ. Based on Figure 11, there was an increase in the elasticity value sequentially from the AZ-1, AZ-2, AZ-3, and AZP-1, AZP-2, and AZP-3 materials. The tensile strength of the AZ and AZP material increased with relatively

regular increments from AZ-1 to AZ-3 and AZP-1 to AZP-3. The regularity of the increase in the tensile strength value could be affected by the gradual addition of ZnO nanoparticles into the sodium alginate solution. In addition, the difference in tensile strength values between sample sheets could be due to the inhomogeneity in AZ material dispersion (Chiang & Chu, 2015; Wang *et al*., 2016). Therefore, some sample sheets differed significantly in AZP material. The inhomogeneity in the AZP material dispersion could be influenced by the difference in tensile strength values between sample sheets.

The AZ-2 had a tensile strength value closest to the average value of the mechanical resistance properties of the AZ material. If we plot the linear line, x (E yield) and y (F yield) were at points 2.2 and 325.17. The converted tensile strength and elasticity value were 17.83 MPa. Likewise, the converted elasticity value could be obtained by plotting a line to determine the E and F yields. The AZ-3 had an elasticity closest to the average value of elasticity AZ 1152.21 MPa. The linear line plot (E yield, F yield) of the AZ-3 was at points 1.4 and 270.25. After the tensile strength value was converted into MPa units, the elasticity value of the AZ-3 was 1364.35 MPa. As with AZ materials, AZP materials displayed varying mechanical resistance properties

The AZP-3 had a tensile strength value closest to the average value of the mechanical resistance properties of the AZP material that had an E yield and F yield of 2.00 and 260.35, respectively. The converted tensile strength and elasticity value were 24.75 MPa. The converted elasticity value could be obtained by plotting a linear line to determine the E and F yields. The AZP-2 was the closest to the average elasticity value of AZP material which was 1160.42 MPa. The linear line plot (E yield, F yield) of the AZP material with sample AZP-3 was at points 1.8 and 400.00. After the tensile strength value was converted into MPa units, the elasticity value of the AZP material was obtained with sample AZP-3 of 11368.68 MPa.

The AZ material had an average tensile strength of 18.08 MPa, whereas the AZP material exhibited a higher average tensile strength performance of 26.8 MPa. Likewise, with the elasticity value, the AZP material performed a greater elasticity value than the AZ material. PEGDMA interpenetration into AZ could increase tensile strength and the AZP material's elasticity. ZnO nanoparticles keep the network stable and effective in the polymer chain. At the same time, PEGDMA strengthens the crosslinking network in the IPN chain (J. Wang *et al*., 2016). In general, IPN materials performed higher tensile strength compared with hydrogel blends. The development of the IPN study of modified alginate and PEG displayed a tensile strength of 2 MPa (Chiang & Chu, 2015). Modified IPN from agarose-ZnO-PEGMA material gave a tensile strength of 1.98–24.8 MPa (Wang *et al*., 2016). Meanwhile, the IPN material from biopolymers had a much lower tensile strength, as in a study using alginate–collagen, which only had a tensile strength of 50–1200 Pa (Branco da Cunha *et al*., 2014). Some related studies have not provided detailed information about the mechanical resistance properties of the material (Lee & Mooney, 2012).

**Study of the antibacterial properties of the AZP material**

The study of the antibacterial properties was initiated by testing ZnO (1) and (2) nanoparticles (Figure 6). ZnO antibacterial test was carried out using the Kirby–Bauer method against bacteria commonly found in wounds, *S. aureus* and *E. coli* (Sehmi *et al*., 2015, 2016). Previous studies reported the results of a descriptive analysis of post-cesarean section patient wounds, which found 59.3 % *S. aureus* and 15.6% *E. coli* (Aditya & Dirgagita, 2021). In addition, Warganegara *et al*. (2012) reported that *E. coli* is one of the bacteria that causes nosocomial surgical wound infections (ILO), found about 19.44% (Warganegara *et al*., 2012). This study used variations in the concentration of ZnO (1) and (2) nanoparticles.

The results show that all AZ and AZP materials could inhibit the bacteria (Table V in Supplementary Materials). Figure 6a displays the percentage of inhibition of AZ and AZP against *S. aureus*. Sequentially, the percentage inhibition for AZ and AZP from the highest to the lowest was AZ-3, AZ-2, AZ-1, AZP-3, AZP-1, and AZP-2. Figure 6b displays the percentage of inhibition of AZ and AZP against *E. coli*. Sequentially, the percentage of inhibition for AZ and AZP from the highest to the lowest was AZ-3, AZ-2, AZ-1, and AZP-3, AZP-2, and AZP-1. The results of the antibacterial properties test for AZ show variations for each bacterium. The inhibition against *S. aureus* showed almost half of the standard percentage for AZ-3. Similar results were reported in the previous studies when ZnO nanoparticles were used as antibacterial agents (Khalid *et al*., 2017; Lam *et al*., 2017).

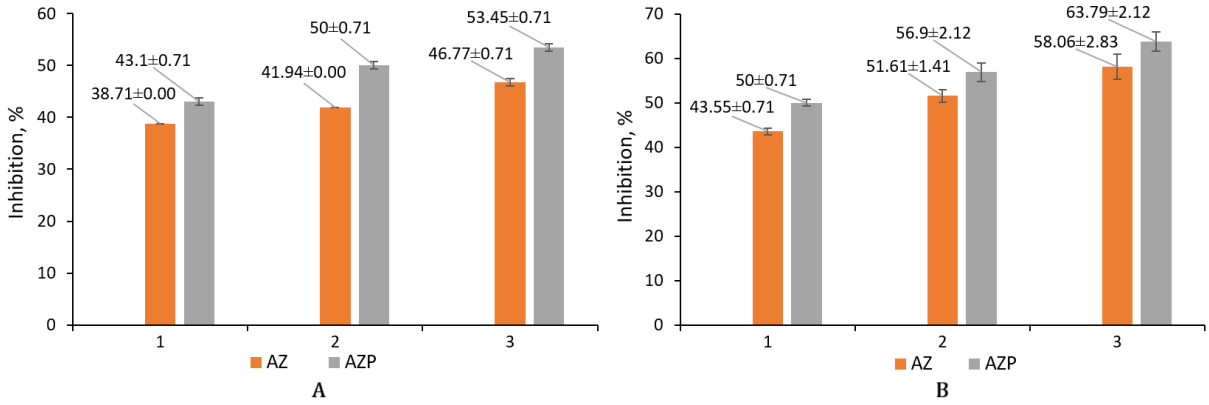


Figure 6. The results of the AZ and AZP antibacterial activity against *E. coli* (a) and *S. aureus* (b)

The percentage of inhibition of AZ against *E. Coli* was 38.71%; 41.94% and 45.16%. While the percentage of inhibition of AZ against *S. aureus* was 41.38%; 48.28% and 51.72%. The percentage of inhibition of Alginate-ZnO-PEGDMA (AZP) against *E. coli* and *S. aureus* each was 45.16%; 54.84%; 64.52% and 62.07%; 64.52%; 68.97%. Previous studies also showed the antibacterial activity of modified ZnO. Modified ZnO with cellulose bacteria showed good antibacterial activity against *P. aeruginosa*, *E. coli,* and *S. Aureus* (Khalid *et al*., 2017). Modifying ZnO with silver showed good antibacterial activity against the growth of *E. coli* bacteria under visible light radiation (Lam *et al*., 2017). The ability of ZnO nanoparticles as antibacterial agents is owing to their crystalline structure, so they are not easily degraded in nature (Khalid *et al*., 2017). In addition, ZnO nanoparticles directly contact the bacteria's cell wall, destroying bacterial cell integrity and increasing ROS formation due to the high amount of oxygen vacancies (Sirelkhatim *et al*., 2015). When it is modified with alginate, which has deficient antibacterial properties, ZnO can increase the antibacterial properties of the material so it can be used as a wound dressing material. Modifying synthetic polymer using PEGDMA with alginate-ZnO as a wound dressing material has not been previously reported. AZP antibacterial activity showed slightly better results compared to AZ. It can be seen from the percentage of inhibition against *E. coli* and *S. aureus*, most of which offer more than 50% of the standards used. Modifying ZnO with agarose and using PEGDMA led to a low percentage of inhibition against *E. coli* and *P. aeruginosa*, below 50% (Wang *et al*., 2016).

## CONCLUSION

AZP material has been successfully synthesized and characterized for its mechanical resistance and antibacterial properties. The mechanical resistance properties were confirmed by the tensile strength and elasticity, which increased about 23.98% and 0.71%, respectively from the origin of AZ. Moreover, the antibacterial activity of AZP against *S. aureus* and *E. coli* increased about 27.71% and 23.53%, respectively, from the origin of AZ. The high mechanical resistance and antibacterial properties of AZP materials make them potentially strong wound dressings.

## REFERENCES

Aditya, R., & Dirgagita, R. (2021). Identification of Bacteria on Postcesarean Section Patient's Wound Operation. *Indonesian Journal of Obstetrics and Gynecology, 9(*1), 38-41.

Al-Sabahi, J., Bora, T., Claereboudt, M., Al-Abri, M., & Dutta, J. (2018). Visible light photocatalytic degradation of HPAM polymer in oil produced water using supported zinc oxide nanorods. *Chemical Engineering Journal*, *351*, 56–64. https://doi.org/10.1016/J.CEJ.2018.06.071

Alavi, M., & Rai, M. (2019). Recent progress in nanoformulations of silver nanoparticles with cellulose, chitosan, and alginic acid biopolymers for antibacterial applications. *Applied Microbiology and Biotechnology*, *103,* 8669 - 8676. https://doi.org/10.1007/s00253-019-10126-4.

Agarwal, A., McAnulty, J. F., Schurr, M. J., Murphy, C. J., & Abbott, N. L. (2011). Polymeric materials for chronic wound and burn dressings. Advanced Wound Repair Therapies. Woodhead Publishing.

Branco da Cunha, C., Klumpers, D. D., Li, W. A., Koshy, S. T., Weaver, J. C., Chaudhuri, O., … Mooney, D. J. (2014). Influence of the stiffness of three-dimensional alginate/collagen-I interpenetrating networks on fibroblast biology. *Biomaterials*, *35*(32), 8927–8936. https://doi.org/10.1016/j.biomaterials.2014.06.047

Chiang, C. Y., & Chu, C. C. (2015). Synthesis of photoresponsive hybrid alginate hydrogel with photo-controlled release behavior. *Carbohydrate Polymers*, *119*, 18–25. https://doi.org/10.1016/J.CARBPOL.2014.11.043

Foliatini, Yulizar, Y., & Hafizah, M. A. E. (2015). The synthesis of alginate-capped silver nanoparticles under microwave irradiation. *Journal of Mathematical and Fundamental Sciences*, *47*(1), 31–50. https://doi.org/10.5614/J.MATH.FUND.SCI.2015.47.1.3

Guo, T. H., Liu, Y., Zhang, Y. C., & Zhang, M. (2011). Green hydrothermal synthesis and optical absorption properties of ZnO2 nanocrystals and ZnO nanorods. *Materials Letters*, *65*(4), 639–641. https://doi.org/10.1016/J.MATLET.2010.11.032

Iwamura, T., Goto, S.-I., Sakaguchi, M., & Chujo, Y. (2016). Synthesis of Submicrometer Zinc Oxide Particles and Zinc Oxide Nanowires Using Microwave Irradiation The Chemical Society of Japan. *Chemical Letter*, *45*(5), 508–510. https://doi.org/10.1246/cl.160081

Jafarirad, S., Mehrabi, M., Divband, B., & Kosari-Nasab, M. (2016). Biofabrication of zinc oxide nanoparticles using fruit extract of Rosa canina and their toxic potential against bacteria: A mechanistic approach. *Materials Science & Engineering. C, Materials for Biological Applications*, *59*, 296–302. https://doi.org/10.1016/J.MSEC.2015.09.089

Khalid, A., Khan, R., Ul-Islam, M., Khan, T., & Wahid, F. (2017). Bacterial cellulose-zinc oxide nanocomposites as a novel dressing system for burn wounds. *Carbohydrate Polymers*, *164*, 214–221. https://doi.org/10.1016/J.CARBPOL.2017.01.061

Khalil, Munawar. (2017). Preparasi sampel nanopartikel koloid untuk karakterisasi dengan menggunakan TEM. Departemen Kimia. Universitas Indonesia.

Lam, S. M., Quek, J. A., & Sin, J. C. (2017). Surfactant-free synthesis of ZnO micro/nanoflowers with efficient photocatalytic antibacterial performance. *Materials Letters*, *195*, 34–36. https://doi.org/10.1016/J.MATLET.2017.02.084

Lam, S. M., Sin, J. C., Zuhairi Abdullah, A., & Rahman Mohamed, A. (2013). Green hydrothermal synthesis of ZnO nanotubes for photocatalytic degradation of methylparaben. *Materials Letters*, *93*, 423–426. https://doi.org/10.1016/J.MATLET.2012.12.008

Lee, K. Y., & Mooney, D. J. (2012). Alginate: properties and biomedical applications. *Progress in Polymer Science*, *37*(1), 106–126. https://doi.org/10.1016/J.PROGPOLYMSCI.2011.06.003

Mahdavi, M., Namvar, F., Ahmad, M. Bin, & Mohamad, R. (2013). Green biosynthesis and characterization of magnetic iron oxide ($Fe_3O_4$) nanoparticles using seaweed (Sargassum muticum) aqueous extract. *Molecules (Basel, Switzerland)*, *18*(5), 5954–5964. https://doi.org/10.3390/MOLECULES18055954

Marinho, J. Z., Romeiro, F. C., Lemos, S. C. S., Motta, F. V., Riccardi, C. S., Li, M. S., … Lima, R. C. (2012). Urea-based synthesis of zinc oxide nanostructures at low temperature. *Journal of Nanomaterials*, *2012*. https://doi.org/10.1155/2012/427172

Mowade, T. K., Dange, S. P., Thakre, M. B., & Kamble, V. D. (2012). Effect of fiber reinforcement on impact strength of heat polymerized polymethyl methacrylate denture base resin: in vitro study and SEM analysis. *The Journal of Advanced Prosthodontics*, *4*(1), 30–36. https://doi.org/10.4047/JAP.2012.4.1.30

Nurbayasari, R., Saridewi, N. & Shofwatunnisa, S. (2017). Biosynthesis and Characterization of ZnO Nanoparticles with extract of Green Seaweed *Caulerpa sp. Jurnal Perikanan Universitas Gadjah Mada*, 19(1), 17-28. https://doi.org/ 10.22146/jfs.24488

Pavlina, E.J. & Tyne, C.J.V. (2008). Correlation of Yield Strength and Tensile Strength with Hardness for Steels. *Journal of Materials Engineering and Performance,* 17, 6.

Romadhan, M. F., Suyatma, N. E., & Taqi, F. M. (2016). Synthesis of ZnO Nanoparticles by Precipitation Method with Their Antibacterial Effect. *Indonesian Journal of Chemistry*, *16*(2)*,* 117 - 123.

Schwartz, A. J., KUmar, M., Adams, B. L. & Field, D. P. (2009). *Electron backscatter diffraction in materials science*. Second edition. Springer.

Sehmi, S. K., Noimark, S., Bear, J. C., Peveler, W. J., Bovis, M., Allan, E., … Parkin, I. P. (2015). Lethal photosensitisation of Staphylococcus aureus and Escherichia coli using crystal violet and zinc oxide-encapsulated polyurethane. *Journal of Materials Chemistry B*, *3*(31), 6490–6500. https://doi.org/10.1039/C5TB00971E

Sehmi, S. K., Noimark, S., Pike, S. D., Bear, J. C., Peveler, W. J., Williams, C. K., … MacRobert, A. J. (2016). Enhancing the Antibacterial Activity of Light-Activated Surfaces Containing Crystal Violet and ZnO Nanoparticles: Investigation of Nanoparticle Size, Capping Ligand, and Dopants. *ACS Omega*, *1*(3), 334–343. https://doi.org/10.1021/ACSOMEGA.6B00017

Shalumon, K. T., Anulekha, K. H., Nair, S. V., Nair, S. V., Chennazhi, K. P., & Jayakumar, R. (2011). Sodium alginate/poly(vinyl alcohol)/nano ZnO composite nanofibers for antibacterial wound dressings. *International Journal of Biological Macromolecules*, *49*(3), 247–254. https://doi.org/10.1016/J.IJBIOMAC.2011.04.005

Sirelkhatim, A., Mahmud, S., Seeni, A., Kaus, N. H. M., Ann, L. C., Bakhori, S. K. M., Hasan, H, & Mohamad, D. (2015). Review on Zinc Oxide Nanoparticles: Antibacterial Activity and Toxicity Mechanism. *Nano-Micro Letters, 7*, 219 - 242. https://doi.org/10.1007/s40820-015-0040-x.

Sun, F., Nordli, H. R., Pukstad, B., Gamstedt, E. K., & Carrasco, G. C. (2017). Mechanical characteristics of nanocellulose-PEG bionanocomposite wound dressings in wet conditions. *Journal of the Mechanical Behavior of Biomedical Materials, 69*, 377 - 384. https://doi.org/10.1016/j.jmbbm.2017.01.049.

Vasquez, R. D., Apostol, J. G., de Leon, J. D., Mariano, J. D., Mirhan, C. M. C., Pangan, S. S., … Zamora, E. T. (2016). Polysaccharide-mediated green synthesis of silver nanoparticles from Sargassum siliquosum J.G. Agardh: Assessment of toxicity and hepatoprotective activity. *Open Nano*, *1*, 16–24. https://doi.org/10.1016/J.ONANO.2016.03.001

Wang, F., Lu, X., & Li, X. Y. (2016). Selective removals of heavy metals (Pb(2+), Cu(2+), and Cd(2+)) from wastewater by gelation with alginate for effective metal recovery. *Journal of Hazardous Materials*, *308*, 75–83. https://doi.org/10.1016/J.JHAZMAT.2016.01.021

Wang, J., Hu, H., Yang, Z., Wei, J., & Li, J. (2016). IPN hydrogel nanocomposites based on agarose and ZnO with antifouling and bactericidal properties. *Materials Science & Engineering. C, Materials for Biological Applications*, *61*, 376–386. https://doi.org/10.1016/J.MSEC.2015.12.023

Warganegara, E., Apriliana, E., & Ardiansyah, R. (2012). Identifikasi Bakteri Penyebab Infeksi Luka Operasi (ILO) Nosokomial Pada Ruang Rawat Inap Bedah Dan Kebidanan Rsam Di Bandar Lampung. *Prosiding SNSMAIP III.*